Material Selection Methodology for an Induction Welding Magnetic Susceptor based on Hysteresis Losses

*Romain Georges Martin, Christer Johansson, Jason Robert Tavares, Martine Dubé**

R. G. Martin, Prof. M. Dubé
CREPEC, Mechanical Engineering, Ecole de Technologie Supérieure (ETS)
1100, rue Notre-Dame Ouest, H3C 1K3, Montréal, Canada
E-mail: martine.dube@etsmtl.ca

Prof. C. Johansson
RISE Research Institutes of Sweden
Arvid Hedvalls Backe 4, SE-411 33, Göteborg, Sweden

Prof. J. R. Tavares
CREPEC, Chemical Engineering, Polytechnique Montréal
2500, chemin de la Polytechnique, H3T 1J4, Montréal, Canada

Keywords: Induction welding, Magnetic susceptor, Hysteresis losses

Abstract

Induction welding is a fusion bonding process relying on the application of an alternating magnetic field to generate heat at the joining interface. This study investigates magnetic hysteresis losses heating elements, called susceptors, which are made of magnetic particles dispersed in a thermoplastic polymer. We propose a methodology to identify the parameters influencing the heating rate of the susceptors and to select suitable magnetic particles for their fabrication. The applied magnetic field amplitude is modelled based on the induction coil geometry and the alternating electrical current introduced to it. Then, properties of the evaluated susceptor particles are obtained through measurements of their magnetic hysteresis. A case study is presented to validate the suitability of the proposed methodology. Particles of iron (Fe), nickel (Ni) and magnetite (Fe_3O_4) are evaluated as susceptor materials in polypropylene (PP) and polyetheretherketone (PEEK) matrices. Heating rates are predicted using the proposed method, and samples are produced and heated by induction to experimentally verify the results. Good agreement with the predictions is obtained. Ni is the most suitable susceptor material for a PP matrix, while Fe_3O_4 is preferable for PEEK.

1. Introduction

The growing demand for thermoplastic composites in different fields such as aerospace has highlighted the need for techniques allowing their reliable and efficient assembly. Fusion bonding (or welding) offers an alternative to mechanical fastening and adhesive bonding for joining thermoplastic composites. Welding relies on the capability of thermoplastics to melt and flow to create a bond under pressure and solidify after cooling [1]–[5]. A few processes – ultrasonic, resistance and induction welding – are of particular interest for the aerospace industry. Among them, induction welding relies on the conversion of an electromagnetic field into heat using an implant, or heating element, called a susceptor. It is a fast process [1] which can be automated and adapted to complex geometries [3].

There are two major heat dissipation mechanisms exploited by susceptor materials: eddy currents and magnetic hysteresis. Eddy currents are induced in electrically-conductive materials subjected to a time-variable magnetic field (**Figure 1a**). They consist in electrical current closed loops which dissipate heat by resistive heating, also defined as Joule losses [6]–[8]. When electrically-conductive carbon fibre-based composites are to be welded, the eddy currents can be induced directly in the adherents, without the need for a susceptor. Direct heating of the carbon fibre works best for fabrics, which provide the closed loops required for the eddy currents generation. When direct heating of the carbon fibre is not possible or if another composite material is used (e.g. glass fibre-based composites), an electrically-conductive susceptor is required at the weld interface, as schematized on **Figure 1b** [8]–[10]. The two main limitations of this heating mechanism are the need for continuity in the susceptor to achieve the creation of current loops and, when directly heating the adherents' carbon fibre, the magnetic shielding, which concentrates the electrical currents, and thus heating, close to the outer adherent's surface [7].

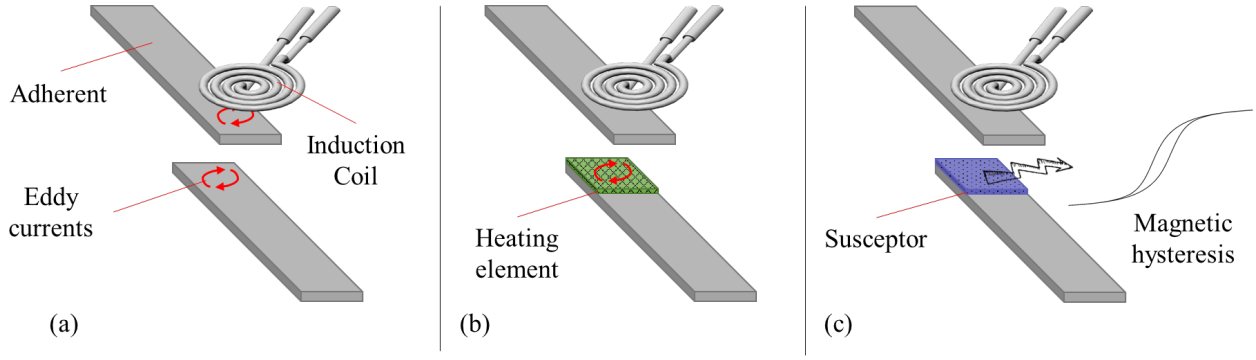

Figure 1. Schematic representation of heat dissipation in induction welding. (a) eddy currents induced directly in an electrically-conductive adherent. (b) eddy currents induced in an electrically-conductive susceptor. (c) heat dissipated by hysteresis losses in a magnetic susceptor.

Alternatively, magnetic hysteresis exploits the property of ferromagnetic materials to dissipate heat when subjected to an alternating magnetic field. Magnetic hysteresis is observed in a susceptor because of the change in the material magnetization; a small amount of energy is dissipated into heat during every single hysteresis loop through magnetic hysteresis losses [11]. To exploit magnetic hysteresis in welding (**Figure 1c**), the susceptor is typically made of ferromagnetic micro- or nanoparticles dispersed into a thermoplastic polymer film [12]–[14].

The heating power of various ferromagnetic particles was investigated by Wetzel and Fink, who defined the heating rate equation explored further in this article [15], [16]. They explored the theoretical heating capability of nickel (Ni), a hard ferrite (Strontium-ferrite) and a soft ferrite (Nickel-Zinc-ferrite). Based on this work, Suwanwatana et al. used Ni particles ranging from 79 nm to 22 µm into polysulfone (PSU) to demonstrate the feasibility of hysteresis heating and its application to weld polyphenylene sulfide (PPS) based composites [12], [17]. Bae et al. conducted a similar study and measured the heating capability of another magnetic material, iron (Fe) particles (8 to 74 µm), dispersed in thermoplastic polyurethane (TPU) adhesives [13]. These two materials were also present among different particulate materials (carbon black, magnetite (Fe_3O_4), Ni and Fe) that Bayerl et al. explored when mixed with high-density

polyethylene (HDPE) [14]. Finally, Stokes used Emaweld products without disclosing the nature of the ferromagnetic particles dispersed in various thermoplastic matrices [3]. They all concluded on the susceptor material efficiency based on the experimental results. In these different studies, no proper justification is provided for selecting one susceptor material over another. In addition, the reported results are valid for a given thermoplastic matrix and a specific induction heating setup.

The goal of this work is to present a more general methodology to predict the heating capacity of ferromagnetic particles dispersed in a thermoplastic polymer, for a given induction heating equipment. To evaluate the heating capability of a susceptor, its initial heating rate, i.e. the heating rate at room temperature, is considered. A method is proposed to select a susceptor material with the highest initial heating rate and the ability to reach a pre-determined temperature corresponding to thermoplastic polymer processing temperature. This approach is applied to a case study in which three potential ferromagnetic materials (Fe, Ni and Fe_3O_4) are evaluated as susceptor candidates. Predicted heating rates are verified experimentally to assess the suitability of the material selection methodology.

2. Methodology for susceptor materials selection and heating rate prediction

2.1 Heating rate equation

Wetzel and Fink proposed a governing equation to express the heating rate of a magnetic susceptor under adiabatic conditions [15]:

$$\frac{dT}{dt} = f E_h \left(\rho c_p + \left(\frac{1}{v_f} - 1 \right) \tilde{\rho} \tilde{c}_p \right)^{-1} \quad (1)$$

with f being the frequency of the alternating magnetic field, E_h the hysteresis absorbed energy density for an applied magnetic field amplitude, v_f the volume fraction of ferromagnetic particles, ρ and $\tilde{\rho}$, the density of the magnetic particles and thermoplastic polymer, respectively,

and c_p and $\tilde{c}_p$, their specific heat capacities. The terms ρc_p and $\tilde{\rho}\tilde{c}_p$ are the volumetric heat capacity of the magnetic particles and thermoplastic polymer, respectively. **Equation (1)** can be used to predict the heating rate of a given susceptor material, and hence identify the most efficient ferromagnetic material to use as a susceptor.

2.2 Magnetic field generation

The first parameters that must be known for the susceptor material selection are the frequency, amplitude and shape of the generated magnetic field. These parameters depend on the material and geometry of the coil and the intensity I and frequency f of the alternating electrical current circulating in it. The coil is generally a water-cooled copper tube, whose geometry has a significant impact on the magnetic induction field amplitude [3]. Various shapes and sizes of coil exist, and they must be chosen to comply with the application and weld geometry [18]–[20].

The amplitude of the magnetic field applied on the susceptor is referred to as H_m. This amplitude depends strongly on the distance between the induction coil and the susceptor (i.e. the coupling distance). The shorter this coupling distance is and the higher the heating rate is. This distance is typically kept under 10 mm [10]–[12], [14], [18], [21].

The coil material properties and its geometry as well as the electrical current intensity and frequency are used to calculate the magnetic field amplitude H_m at any point in space and especially at the joining interface. Finite elements modelling software such as FEMM 4.2 can be used to that end [22]. The H_m value is then used to determine the absorbed energy density E_h.

2.3 Thermoplastic matrix

The susceptor material is composed of ferromagnetic particles dispersed in a thermoplastic matrix, which must be selected to be compatible with the composite adherents to be welded [19].

The glass transition temperature T_g and melting temperature T_m (for semi-crystalline polymers) of the thermoplastic matrix are obtained by Differential Scanning Calorimetry (DSC). The specific heat capacity of the polymer can also be extracted from DSC measurements following the ASTM E1269 standard.

2.4 Ferromagnetic particles

The main part of the susceptor material selection is the choice of the ferromagnetic particles. The density ρ and specific heat c_p of the material must be known. When subjected to an alternating magnetic field of frequency f, magnetic materials experience a magnetization whose direction will alternate at a similar frequency. The magnetization of ferromagnetic materials (e.g. cobalt (Co), Fe, Ni) lags behind the applied field, causing a magnetic hysteresis visible on the B-H curve (**Figure 2**), with H being the applied magnetic field and B the magnetic induction of the magnetic material.

The absorbed energy density per hysteresis loop and per unit volume E_h is determined as:

$$E_h = \mu_0 \oint H dB \tag{2}$$

and corresponds to the enclosed surface area (in grey in Figure 2) [24]. The magnetic permeability of vacuum μ_0 is equal to $4\pi \cdot 10^{-7}$ H m^{-1}. During every single loop of hysteresis, an amount of energy equal to the absorbed energy density E_h is dissipated into heat [25]. The dissipated power per unit volume is thus obtained by multiplying the absorbed energy density E_h by the frequency f:

$$P_h = f E_h \tag{3}$$

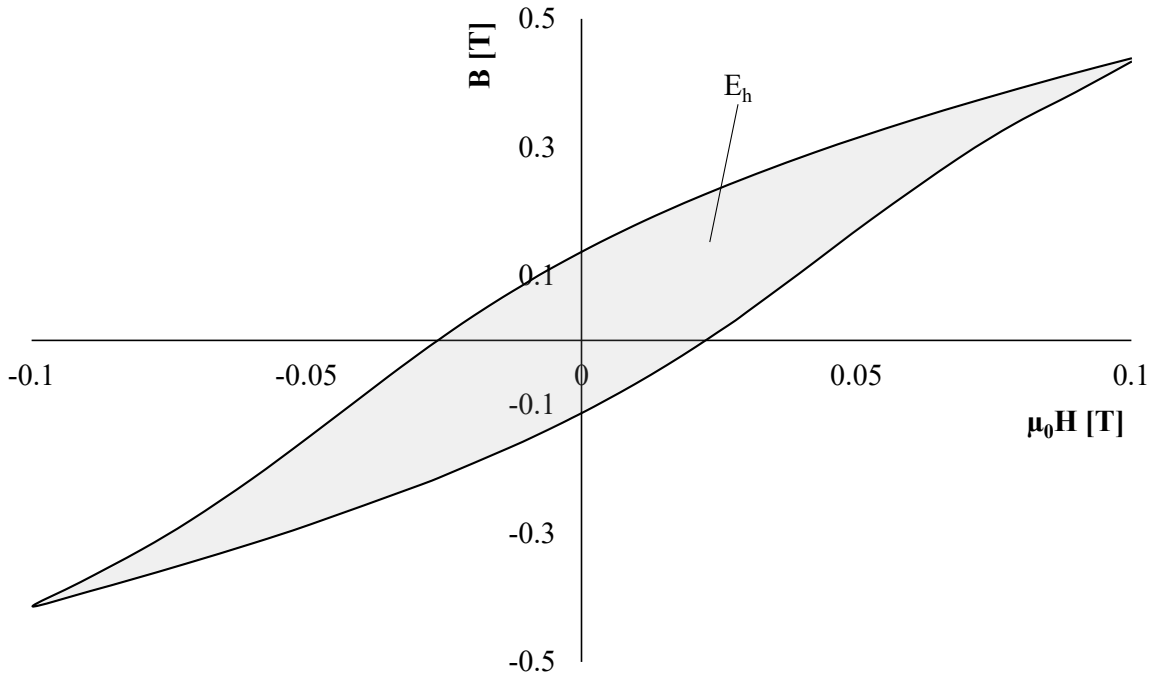

Figure 2. Hysteresis curve of a ferromagnetic material (magnetic induction B as a function of applied field H). The enclosed surface area (in grey) corresponds to the absorbed energy density E_h.

Predicting E_h for given values of H_m is challenging. It can be done using the Steinmetz equation (classic and generalized [25]–[28]), although its parameters are defined empirically and it is valid at low field amplitudes only (i.e. when the applied field amplitude H_m is largely smaller than the saturation field at which the material reaches its saturation magnetization). The best way to obtain E_h versus H_m is through Vibrating Sample Magnetometer (VSM) measurements for various field amplitudes and extrapolate the curve from the results [24]. If the experimentally applied field amplitude H_m is known, then only the hysteresis for that applied field is to be measured by VSM to extract the corresponding value of E_h for the magnetic material.

2.5 Curie temperature

Ferromagnetic materials exhibit temperature-dependent magnetic properties. As temperature increases, the material gradually loses its properties, until it reaches the Curie point (noted T_c) where they disappear [24], [29]. The Curie temperatures of magnetic materials are well-documented in the literature [23], [29].

Susceptor materials used in induction welding must have their T_c above the polymer processing temperature, as heating of the ferromagnetic particles is interrupted at T_c:

$$T_{c,particles}\ [K] > T_{process,thermoplastic}\ [K] + 10\% \quad (4)$$

A 10% margin is suggested as the magnetic properties of the ferromagnetic particles decrease when approaching T_c, leading to reduced heating capabilities. When $T = 0.9T_c$, the remaining magnetization is approximately 50% of its maximum value [23], corresponding to the lower limit ensuring efficient heating.

In some cases, susceptor materials can be selected so that T_c is above the polymer melting point but below the polymer degradation temperature. The susceptor is then used as a thermal control feature capable of melting the polymer and stop heating before degrading it. Unfortunately, T_c of ferromagnetic materials vary over a large range, from a few dozen degrees to over 1000 K. Finding a susceptor material exhibiting a T_c within the polymer's processing window is sometimes impossible.

2.6 Methodology summary

The presented methodology is summarized in **Table 1**. As explained, the three main steps are the characterization of the applied magnetic field using a finite element modelling software, the thermoplastic polymer thermal and physical properties using DSC and material technical

datasheet (TDS), and the magnetic particles magnetic, thermal and physical properties using VSM measurements and material TDS. The Curie temperature of the evaluated magnetic particles must satisfy the criterion presented in **Equation (4)**. Once all the required parameters are characterized, the heating rate can be predicted using Equation (1).

Table 1. Susceptor material selection methodology summary.

	1. Magnetic field	**2.Thermoplastic polymer**	**3. Magnetic particles**
Parameters to define/characterize	H_m, f	T_m (or T_g), $T_{process}$, $\tilde{\rho}$, $\tilde{c}_p$	E_h, ρ, c_p, T_c, v_f
Method	Magnetic field modelling	DSC, TDS	VSM, TDS
T_c criterion	-	$T_{c,particles}\,[K] > T_{process,thermoplastic}\,[K] + 10\%$	
	↓	↓	↓
Heating rate prediction	$\frac{dT}{dt} = f E_h \left(\rho c_p + \left(\frac{1}{v_f} - 1\right)\tilde{\rho}\tilde{c}_p\right)^{-1}$		

3 Case study

Three potential ferromagnetic materials for an induction welding susceptor film are evaluated as a case study, following the presented methodology (Table 1). The considered materials are Fe, Ni and Fe_3O_4. Two semi-crystalline thermoplastics are evaluated: a commodity polymer, polypropylene (PP), and a high-performance polymer, poly-ether-ether-ketone (PEEK). In the first part of the case study, the heating rates of the susceptors are predicted using the presented approach. In the second part, susceptor samples are prepared and the heating rate predictions are compared with experimental results to verify the method.

3.1 Heating rate prediction

3.1.1 Induction heating equipment

Induction heating is performed using an Ambrell EASYHEAT 10kW power supply (maximum current 750 A with a frequency range of 150-400 kHz). A hairpin coil is mounted on the induction working head. The intensity of the alternating current travelling through the induction coil is fixed at 700 A. The frequency is automatically calculated by the generator software to reach the LC resonance frequency of the induction coil, based on the following formula:

$$f = \frac{1}{2\pi\sqrt{LC}} \tag{5}$$

with L being the inductance of the coil and C the capacitance of the generator. For the present experiments, two 2 μF capacitors are mounted in series in the work head, providing a total capacitance C = 1 μF. Together with the inductance of the coil L = 0.35 μH, the resonance frequency is calculated by the generator to be 269 kHz. Induction experiments are conducted at that frequency.

The induction coil is equipped with a Ferrotron 559H magnetic field concentrator from Fluxtrol. The induction magnetic field around the hairpin coil and the field concentrator is calculated using the FEMM4.2 software [22], as presented in **Figure 3a**. Details about the finite element model are available in the supporting information. The absolute value of the intensity of the induced magnetic field density H when located 5 mm away from the coil is shown in **Figure 3b**. The maximum intensity H_m is 32 kA m^{-1} (0.04 T) at 700 A and 269 kHz. An assumption is made that the presence of the magnetic susceptor does not impact the magnetic field lines.

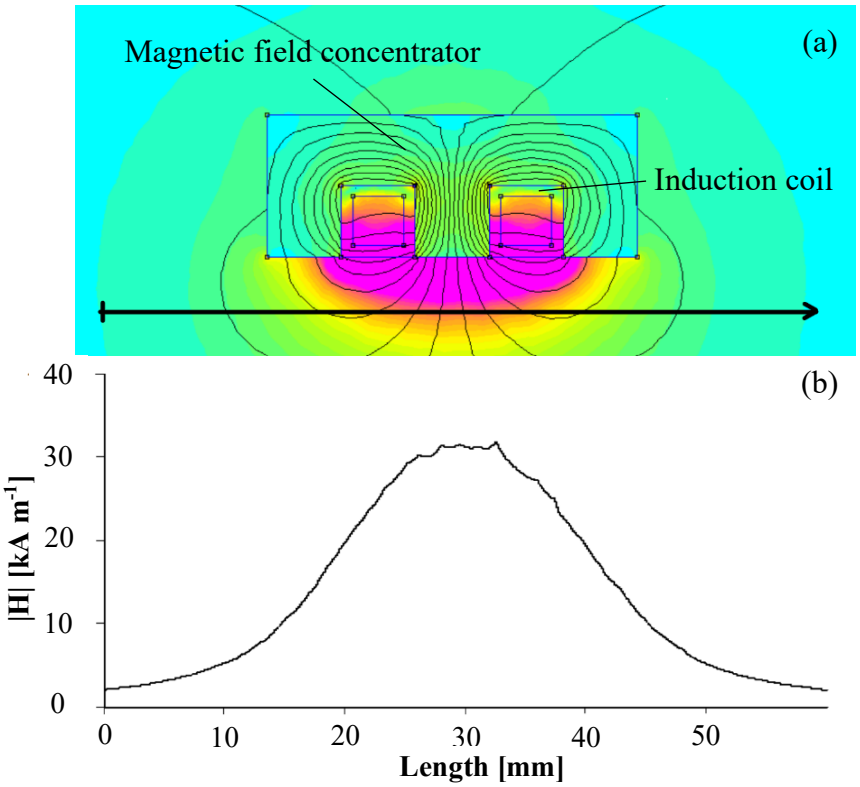

Figure 3. Magnetic field density simulation around a hairpin water-cooled copper coil equipped with a Ferrotron 559H field concentrator, with a 700 A current at 269 kHz. (a) Field amplitude in a profile perpendicular to the coil axis. Black arrow corresponds to the sample location, 5 mm away from the coil. The color code scales from light blue (<2kA/m) to purple (>40kA/m) with increments of 2kA/m. (b) Field amplitude along the black arrow. Center of the coil is located at 30 mm on the x-axis.

3.1.2 Materials

PEEK (grade 90G from Victrex) and PP (grade 1104A from Pinnacle Polymers) densities are 1300 kg m^{-3} and 900 kg m^{-3}, respectively. Their melting points and recrystallisation temperatures are obtained by DSC with heating and cooling rates of 10 °C min^{-1}, as presented in **Figure 4** and reported in **Table 2**. Their room temperature specific heat capacities are calculated from the DSC curves and are reported in Table 2.

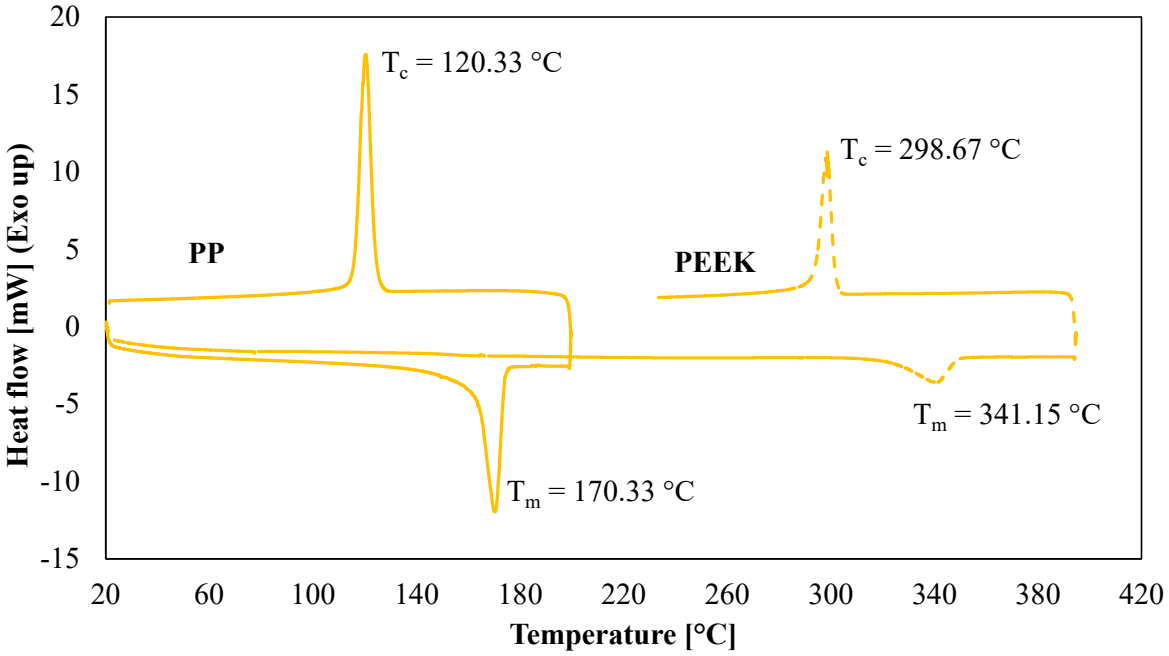

Figure 4. Heating and cooling DSC curves for PP (solid line) and PEEK (dashed line). The bottom peaks correspond to the melting of the polymer and the top peaks to the recrystallisation. The melting and recrystallisation temperatures are shown next to each peak.

Table 2. PP and PEEK specific heat capacity, melting point and recrystallisation temperature, as measured by DSC.

Material	Specific heat capacity at 25 °C [J kg^{-1} K^{-1}]	Melting point [°C]	Recrystallisation temperature [°C]
PP 1104A	1970	170	120
PEEK 90G	1140	341	299

Fe, Ni and Fe_3O_4 particles are well-known for their magnetic properties. Fe has a small coercivity and is typically classified as a soft magnet [30]. Fe_3O_4 is classified as a hard ferrite and therefore exhibit a larger coercivity and hysteresis curve [31]. Ni's magnetic properties are intermediate [15]. In general, materials with large coercivity exhibit large magnetic hysteresis. The goal of this methodology is to evaluate which of the three candidates can provide the highest heating rate when used as a susceptor under the described experimental conditions.

The particles diameter, density and specific heat capacity are summarized in **Table 3**, along with their T_c. All particles, including Fe_3O_4, have large enough diameters so that their magnetic properties fall in the multi-domain region. Fe_3O_4's critical diameter at which the material is in a single domain region and the coercivity is maximum is around 80 nm [32]–[35].

Table 3. Magnetic particles suppliers, mean diameters and densities (from materials technical data sheets), and specific heat capacities and Curie temperatures (from literature).

Material	Supplier	Particles mean diameter [µm]	Density [kg m^{-3}]	Specific heat capacity [J kg^{-1} K^{-1}]	Curie temperature [°C]
Fe	US Research Nanomaterials Inc.	45	7874	448 [36]	768 [11]
Ni	Sigma-Aldrich	50	8900	443 [36]	358 [11]
Fe_3O_4	Höganäs AB	0.8	5170	647 [37]	575 [11]

3.1.3 Hysteresis curves

The magnetic hysteresis *B-H* curves of the three magnetic particles are measured, using a VSM model 7307 (Lakeshore Cryotronics). The maximum applied field H_m varies from 16 to 32, 40, 48, 64 and 80 kA m^{-1} (0.02, 0.04, 0.05, 0.06, 0.08 and 0.1 T). The absorbed energy density E_h of the three susceptor materials under these field amplitudes is calculated using equation (2) and reported in **Figure 5**. The corresponding hysteresis of Fe, Ni and Fe_3O_4 under H_m = 32 kA m^{-1}, the calculated field amplitude in the inductor, are presented in **Figure 6**. Ni presents the largest measured enclosed surface area (2200 J m^{-3}), with approximately 50% more absorbed energy than Fe_3O_4 (1500 J m^{-3}). Fe exhibits a small hysteresis and small coercivity and negligible enclosed surface area. These properties indicate that Fe particles cannot dissipate a large quantity of heat and thus are a poor magnetic susceptor.

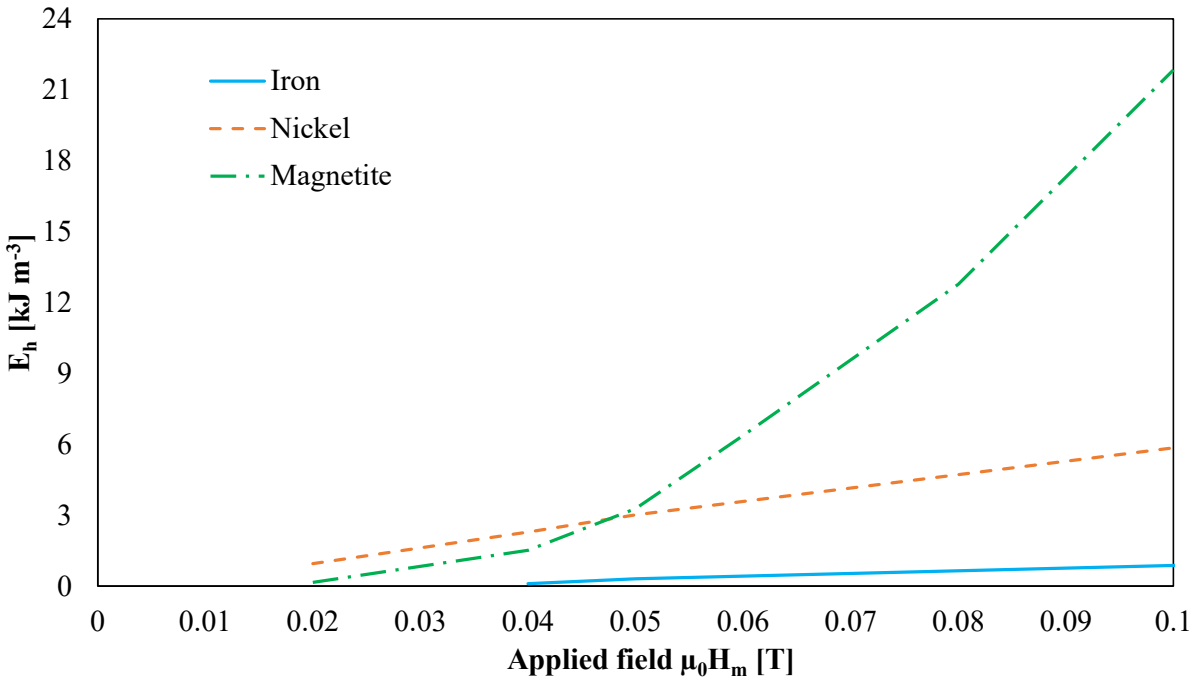

Figure 5. Absorbed energy density versus the applied field amplitude for Fe, Ni and Fe_3O_4 particles.

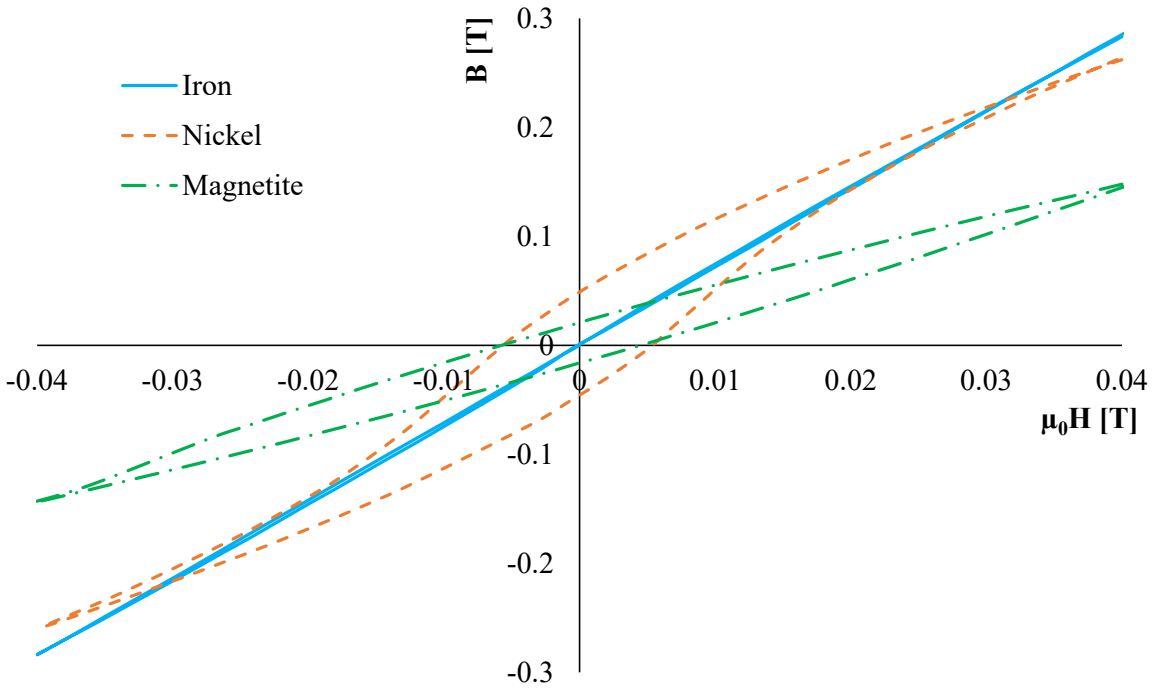

Figure 6. Hysteresis curves (B versus $\mu_0 H$) of Fe, Ni and Fe_3O_4 particles. The applied field amplitude H_m is 32 kA m^{-1} ($\mu_0 H_m$ = 0.04 T).

3.1.4 Predicted heating rate

Equation (1) is used to calculate the initial heating rate for Fe, Ni and Fe_3O_4, mixed with PP and PEEK (5%vol and 10%vol). It appears clearly in equation (1) that the predicted heating rate is proportional to the absorbed energy density, or the hysteresis enclosed surface area. On this basis, Ni-based susceptor films should exhibit the largest initial heating rate, due to Ni's largest magnetic hysteresis under the applied field density of 32 kA m^{-1}. **Table 4** summarizes the predicted heating rates for PP and PEEK susceptors for the two considered magnetic particles and two volume fractions. The predicted initial heating rates of the PP and PEEK susceptors are similar, which is due to the close volumetric specific heat capacity of the two thermoplastic matrices. However, Ni does not satisfy equation (4) as its Curie temperature (631 K = 358 °C) is lower than the PEEK processing temperature of 380 °C to 400 °C. Therefore, although Ni offers a higher heating rate than Fe_3O_4, it cannot reach the PEEK processing temperature and is not a suitable susceptor for this polymer. We conclude that Ni is a good choice of susceptor for PP (offers higher heating rate than Fe_3O_4 and can reach the PP processing temperature) while Fe_3O_4 is better for PEEK (lower heating rate but can reach the PEEK processing temperature). Fe susceptors should present a negligible heating rate due to hysteresis losses because of the negligible enclosed surface area of Fe's magnetic hysteresis (Figure 6). Their predicted value of initial heating is then set at 0 in Table 4.

Table 4. Predicted initial heating rates for PP- and PEEK-based susceptors, mixed with Fe, Ni and Fe_3O_4 particles, at 5%vol and 10%vol under a 32 kA m^{-1} magnetic field amplitude and a frequency of 269 kHz.

	Predicted initial heating rate [K s^{-1}]			
Polymer	PP		PEEK	
Volume fraction	5%	10%	5%	10%
Ni	15.7	29.7	18.4	34.3
Fe_3O_4	10.9	20.9	12.8	24.2

Fe	0	0	0	0

3.2 Experimental validation

3.2.1 Samples preparation

Susceptor samples are prepared by mixing magnetic particles with either PP or PEEK in a Thermo Scientific HAAKE Minilab II micro-extruder. The polymer is melted at 180 °C (PP) and 370 °C (PEEK) for 5 minutes. The Fe, Ni or Fe_3O_4 particles are then added and mixed with the polymer for 10 minutes, and the resulting mix is extruded. The remaining material inside the machine is also recovered. To ensure a more homogeneous distribution of the particles, the extruded material is melted and mixed again in the micro-extruder, following the same procedure. After this second mixing step, the obtained material is shredded into small pellets and pressed into a 1-mm thick film in a hot press. The polymers are pressed at 180 °C for PP and 370 °C for PEEK under a pressure of 5 MPa for 5 minutes. Two volume ratios, 5% and 10%, are considered for each combination of polymer and magnetic particles. Samples are cut into 4 cm x 4 cm specimens for characterization.

Temperature during induction heating is measured using a Jenoptik IR-TCM HD infrared thermal camera. The maximum temperature measured over the sample is recorded and used to produce the heating curves. To perform an accurate quantitative thermography analysis, the emissivity of the sample is first estimated [38]: the sample is placed on a heating plate, and temperature is monitored with a thermocouple and the thermal camera, set with a default emissivity of 1. The ratio between the two values is the actual emissivity of the sample: 0.9 for both PP-Ni and PEEK-Ni samples, and 0.94 for both the Fe- and Fe_3O_4-based samples. The emissivity value is considered as temperature-independent.

Temperature evolution during induction heating is extracted from the thermal camera using the IRT Analyzer 7 software. The initial heating rate is the largest slope of the curve (i.e. the largest

temperature increase over an elapsed time of 1 s), which typically occurs at the beginning of the heating, as shown in **Figure 7**.

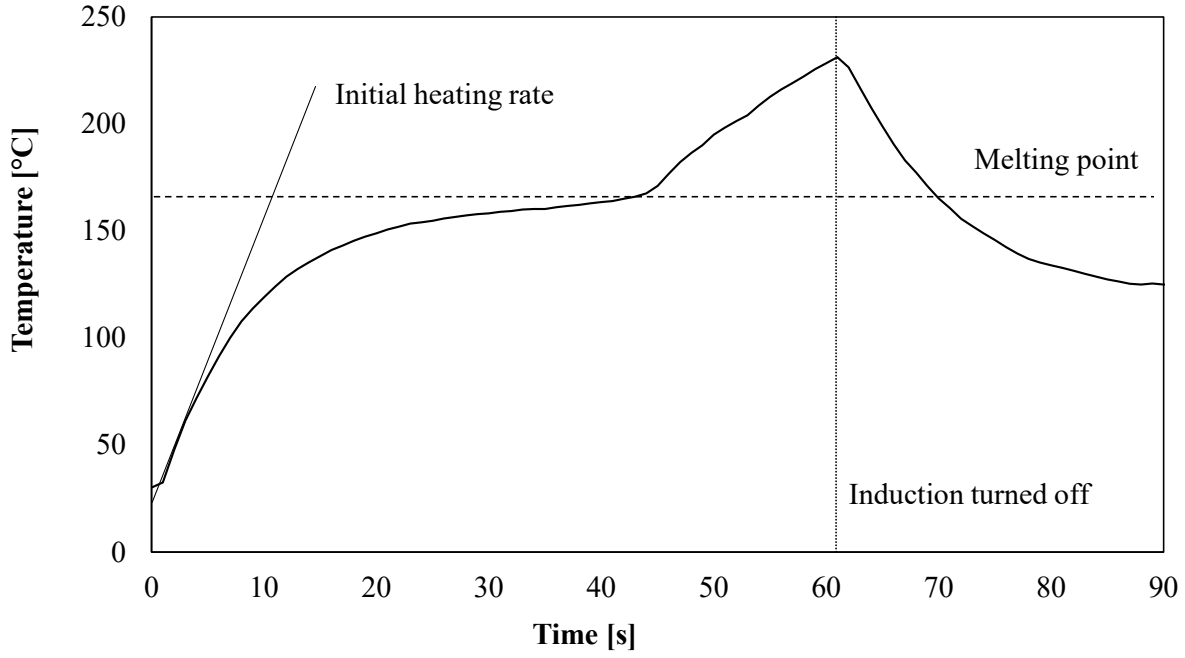

Figure 7. Typical induction heating curve (PP/Ni-5% specimen). The straight-line slope represents the initial heating rate, and the dashed line corresponds to the thermoplastic melting point. The flattening of the curve when approaching the melting temperature is due to the endothermic phase change. Induction heating is turned off after 60 seconds (dotted line).

3.2.2 Experimentally measured heating rates

The temperature evolution of the sample during induction heating is measured using the setup presented in **Figure 8**. The distance between the coil and the sample is fixed at 5 mm. The hairpin coil is equipped with a magnetic field concentrator, as previously explained. The IR camera records the temperature evolution.

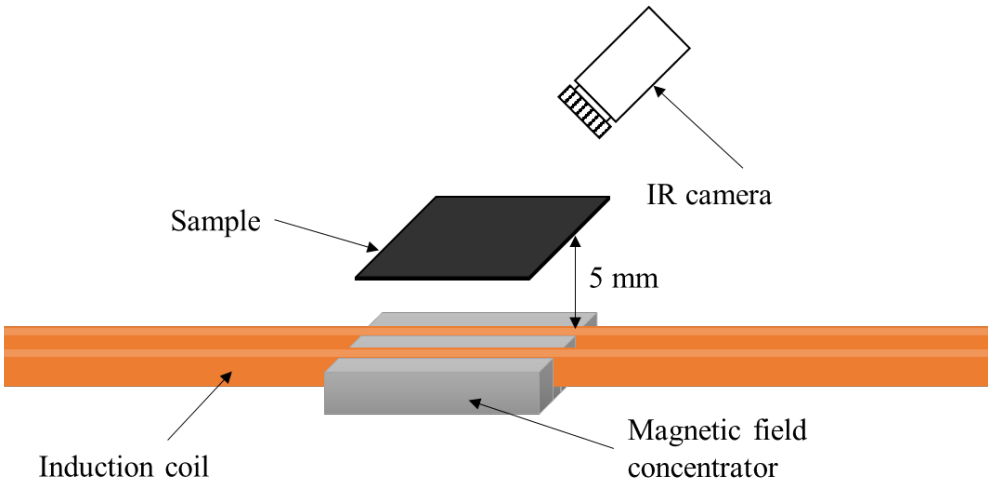

Figure 8. Induction heating setup scheme.

Initial heating rates of PP-based susceptors are presented in **Table 5**. Samples made of Fe, Ni and Fe_3O_4 at volume fractions of 5% and 10% are prepared and four specimens per sample are used. **Figure 9** presents the full heating curves for one representative specimen from each sample. Ni-based susceptors exhibit a larger initial heating rate at both volume fractions, as predicted by the model equation. Experimental values are lower than the model predictions because the model does not consider thermal losses by conduction into the support plate or by convection into the surrounding ambient air. Fe_3O_4-based samples show lower heating rates than Ni-based ones, but they are higher than the predicted values. This is explained by the presence of small hot spots observed during heating, attributed to locally higher volume fraction of Fe_3O_4 than in the rest of the sample. An improved distribution would reduce such occurrences and produce more consistent results. Fe-based samples present the lowest initial heating rates, as expected from the model. The observed heating rates most probably come from the heat dissipated by induced eddy currents in the Fe particles. However, such heating is too small to reach the melting point of PP. In general, as predicted from the model (equation (1)), susceptors made of Ni particles heat faster than Fe_3O_4-based ones.

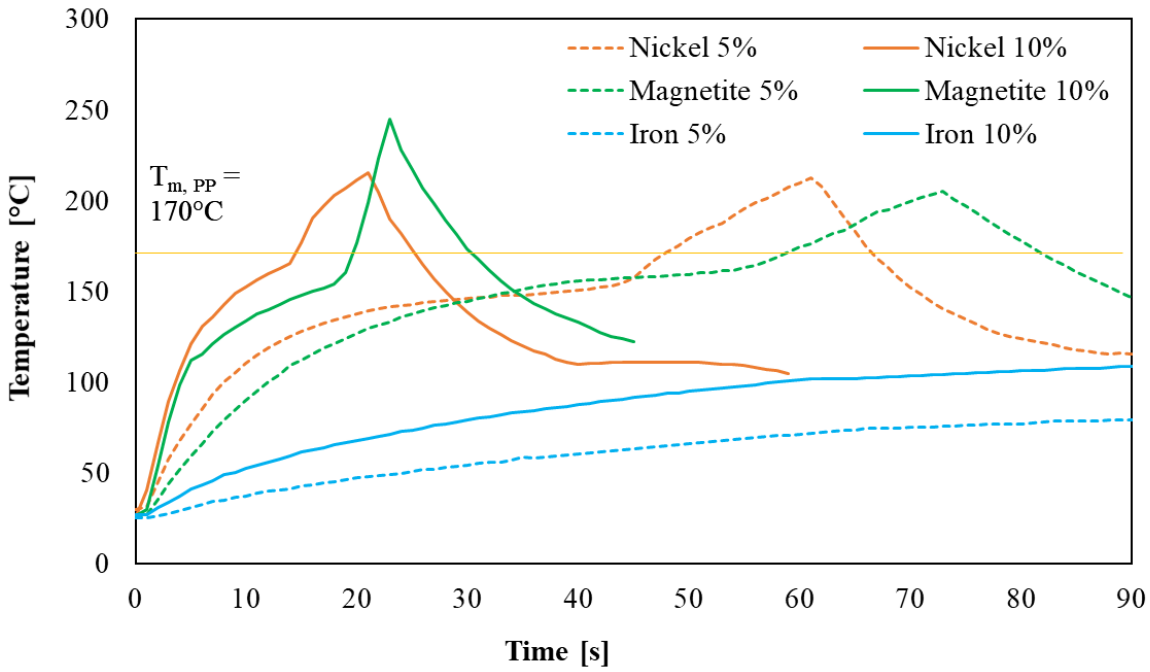

Figure 9. Induction heating of PP-based susceptors (applied magnetic field amplitude of 0.04 T, frequency of 269 kHz). Induction was turned off when reaching 250 °C to avoid sample degradation. Dashed lines correspond to particles concentration of 5%vol and solid lines to 10%vol.

Due to the poor results of the PP/Fe susceptors, Fe is not evaluated with PEEK. The model predicts a larger initial heating rate for PEEK/Ni susceptors, but the T_c of Ni should prevent it from reaching the melting point of PEEK (343 °C). Experimental results confirm this hypothesis; the 5%vol Ni sample only reached 202 °C and the 10%vol sample reached 264 °C. **Figure 10** shows a representative heating curve for each sample. The 5%vol PEEK/Fe_3O_4 sample do not reach the melting point either, showing a maximum measured temperature of 283 °C, likely due to thermal losses in the surrounding air and in the supporting plate. However, the 10%vol PEEK/Fe_3O_4 sample was able to melt PEEK. During this test, induction heating was turned off after 45 seconds to avoid burning the thermoplastic. The results for PEEK-based susceptors also agree with the model prediction, which correctly determined that the favorable magnetic particle material to use is Fe_3O_4.

Table 5. Predicted and measured initial heating rate for PP- and PEEK-based susceptors, mixed with Fe, Ni, and Fe_3O_4 particles, at 5%vol and 10%vol under a 32 kA m^{-1} magnetic field amplitude and a frequency of 269 kHz.

Initial heating rate (Predicted / Measured) [K s^{-1}]				
Polymer	PP		PEEK	
Volume fraction	5%	10%	5%	10%
Ni	15.7 / 13.6	29.7 / 25.7	18.4 / 16.5	34.3 / 28.7
Fe_3O_4	10.9 / 10.6	20.9 / 22.3	12.8 / 9.8	24.2 / 25.1
Fe	0 / 3.0	0 / 3.9	-	-

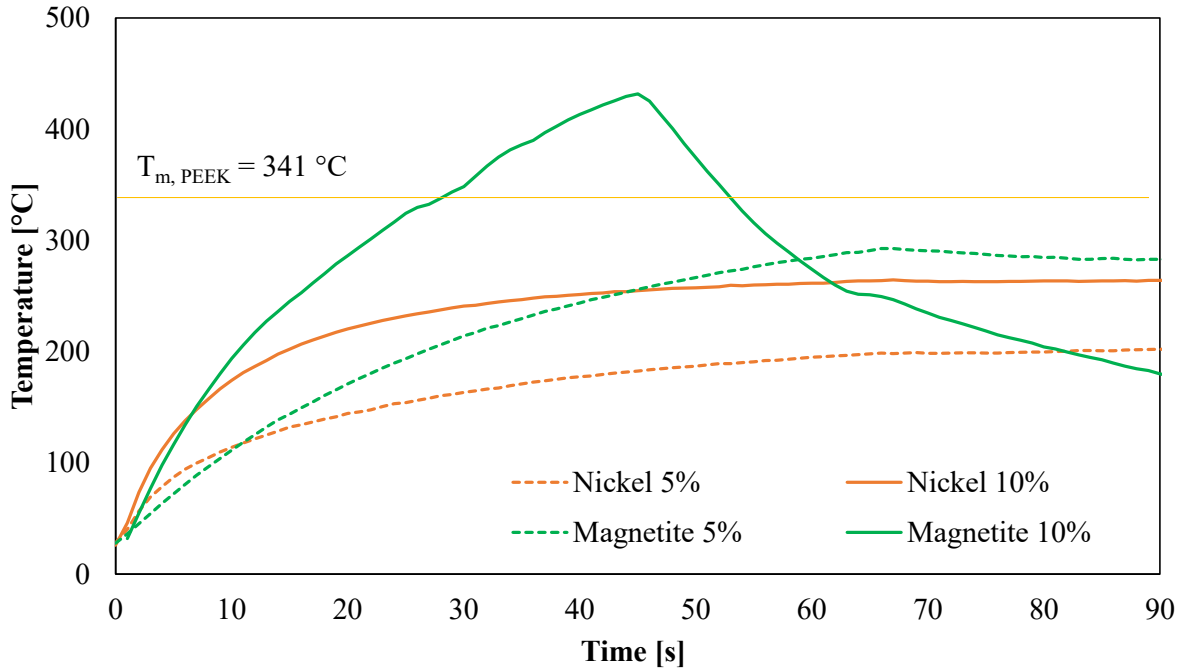

Figure 10. Induction heating of PEEK-based susceptors (applied magnetic field amplitude of 0.04 T, frequency of 269 kHz). Only the PEEK/Fe_3O_4-10%vol sample reached the melting point (solid green curve), for which induction was turned off after 45 seconds. Dashed lines correspond to particles concentration of 5%vol and solid lines to 10%vol.

3.3 Discussion

Experimental results generally show lower heating rates than the model predictions. This can be explained by equation (1) being valid for thermally insulated susceptors, without

consideration for any heat transfer by convection with the surrounding air or by conduction in the samples support. The presented methodology nonetheless provides the correct ranking of the three susceptors heating efficiency, offering engineers a tool to determine which susceptor material is the most suitable for a given thermoplastic matrix and the generator used for induction heating. On a practical note, however, the hardness of Fe_3O_4 presents a processing drawback for the mixing with the thermoplastic matrix. On the Mohs scale, Fe_3O_4 has a hardness ranging from 6 to 6.5 [39], whereas Ni and Fe typically have a hardness of 4 [40]. Mixers are typically made of steel (hardness between 4 and 4.5), meaning that Ni and Fe cannot scratch it, but Fe_3O_4 can. Abrasion was observed on the micro-extruder used during the mixing procedure. Special mixers made of harder materials (e.g. ceramics or hardened steels), should be used to avoid damaging the equipment while mixing Fe_3O_4 with thermoplastic polymers.

Another observation made during the experiments is the apparent phase change that Fe_3O_4 underwent during mixing with PEEK at 380 °C. The dark grey/black color of the Fe_3O_4 particles before mixing became a brown color, similar to rust. This reveals the possible presence of maghemite (γ-Fe_3O_2), which is an intermediate state in the transformation from Fe_3O_4 to hematite (Fe_3O_2) that appears at temperatures around 300-400 °C [41]. The complete transformation into Fe_3O_2 occurs at higher temperature (around 600 °C). γ-Fe_3O_2 has the same atomic structure as Fe_3O_2 but remains in the same crystalline structure as Fe_3O_4, which gives somewhat similar magnetic properties [42]. Its absorbed energy density is considered as equal to the one measured for Fe_3O_4.

4. Conclusion

A methodology was presented to select susceptor materials for the induction welding of thermoplastic composites, with minimal material characterization effort. The proposed methodology can be applied to any combination of magnetic particles and thermoplastic matrices, being a reliable screening tool for material selection of induction welding susceptor

films relying on hysteresis losses for heat generation. The methodology requires knowledge of the magnetic field amplitude that the welding setup can produce, the thermal properties of the matrix and particles used for the susceptor and the magnetic hysteresis of the magnetic particles as measured by VSM.

A case study was presented in which three magnetic particles and two thermoplastic polymers were considered for susceptor manufacturing. The heating rate was predicted based on Wetzel and Fink equation and compared with experimental data. A good agreement was obtained, although the prediction does not consider thermal losses in the environment. Fe presented poor heating rates with PP and therefore was not investigated with PEEK. Ni was shown to be the most appropriate susceptor material to melt PP while Fe_3O_4 was more appropriate for PEEK, due to the low Curie temperature of Ni.

Supporting Information

Supporting Information is available from the Wiley Online Library or from the author.

Acknowledgements

The authors acknowledge financial support from NSERC (Natural Sciences and Engineering Research Council of Canada) (grant number ALLRP 556497 - 20), the Canadian Space Agency (CSA), Ariane Group, Nanoexplore, Mekanic and CREPEC (Centre for Applied Research on Polymers and Composites).

Received: ((will be filled in by the editorial staff))
Revised: ((will be filled in by the editorial staff))
Published online: ((will be filled in by the editorial staff))

References

[1] A. Yousefpour, M. Hojjati, J.-P. Immarigeon, « Fusion Bonding/Welding of Thermoplastic Composites », 2004, doi: 10.1177/0892705704045187.

[2] C. Ageorges, L. Ye, M. Hou, « Advances in fusion bonding techniques for joining thermoplastic matrix composites: A review », *Compos. Part Appl. Sci. Manuf.*, vol. 32, p. 839-857, juin 2001, doi: 10.1016/S1359-835X(00)00166-4.

[3] V. K. Stokes, « Joining methods for plastics and plastic composites: An overview », 1989. doi: 10.1002/pen.760291903.
[4] D. Brassard, M. Dubé, J. R. Tavares, « Resistance welding of thermoplastic composites with a nanocomposite heating element », *Compos. Part B Eng.*, vol. 165, p. 779-784, mai 2019, doi:10.1016/j.compositesb.2019.02.038
[5] D. Brassard, M. Dubé, J. R. Tavares, « Modelling resistance welding of thermoplastic composites with a nanocomposite heating element », *J. Compos. Mater.*, vol. 55, nº 5, p. 625-639, mars 2021, doi: 10.1177/0021998320957055.
[6] T. J. Ahmed, D. Stavrov, H. E. N. Bersee, A. Beukers, « Induction welding of thermoplastic composites—an overview », *Compos. Part Appl. Sci. Manuf.*, vol. 37, nº 10, p. 1638-1651, oct. 2006, doi: 10.1016/j.compositesa.2005.10.009.
[7] L. Moser, « Experimental Analysis and Modeling of Susceptorless Induction Welding of High Performance Thermoplastic Polymer Composites », 2012,
[8] R. Dermanaki Farahani M. Dubé, « Novel Heating Elements for Induction Welding of Carbon Fiber/Polyphenylene Sulfide Thermoplastic Composites », *Adv. Eng. Mater.*, vol. 19, p. e201700294, juin 2017, doi: 10.1002/adem.201700294.
[9] S. Yarlagadda, B. K. Fink, J. J. W. Gillespie, « Resistive Susceptor Design for Uniform Heating during Induction Bonding of Composites »:, *J. Thermoplast. Compos. Mater.*, août 2016, doi: 10.1177/089270579801100403.
[10] R. Dermanaki Farahani, M. Janier, M. Dubé, « Conductive films of silver nanoparticles as novel susceptors for induction welding of thermoplastic composites », *Nanotechnology*, vol. 29, janv. 2018, doi: 10.1088/1361-6528/aaa93c.
[11] T. Bayerl, M. Duhovic, P. Mitschang, D. Bhattacharyya, « The heating of polymer composites by electromagnetic induction – A review », *Compos. Part Appl. Sci. Manuf.*, vol. 57, p. 27-40, févr. 2014, doi: 10.1016/j.compositesa.2013.10.024.
[12] W. Suwanwatana, S. Yarlagadda, J. W. Gillespie, « Hysteresis heating based induction bonding of thermoplastic composites », *Compos. Sci. Technol.*, vol. 66, nº 11, p. 1713-1723, sept. 2006, doi: 10.1016/j.compscitech.2005.11.009.
[13] D. Bae, P. Shin, S. Kwak, M. Moon, M. Shon, S. Oh, G. Kim « Heating behavior of ferromagnetic Fe particle-embedded thermoplastic polyurethane adhesive film by induction heating », *J. Ind. Eng. Chem.*, vol. 30, p. 92-97, oct. 2015, doi: 10.1016/j.jiec.2015.05.007.
[14] T. Bayerl, R. Schledjewski, P. Mitschang, « Induction Heating of Thermoplastic Materials by Particulate Heating Promoters », *Polym. Polym. Compos.*, vol. 20, p. 333-342, mai 2012, doi: 10.1177/096739111202000401.
[15] E. D. Wetzel, B. K. Fink, « Feasibility of Magnetic Particle Films for Curie Temperature-Controlled Processing of Composite Materials », p. 83.
[16] E. D. Wetzel, B. K. Fink, « Adherend Thermal Effects During Bonding with Inductively Heated Films », 2001, doi: 10.21236/ada389305.
[17] W. Suwanwatana, S. Yarlagadda, J. W. Gillespie, « Influence of particle size on hysteresis heating behavior of nickel particulate polymer films », *Compos. Sci. Technol.*, vol. 66, nº 15, p. 2825-2836, déc. 2006, doi: 10.1016/j.compscitech.2006.02.033.
[18] S. Pappadà, A. Salomi, J. Montanaro, A. Passaro, A. Caruso, A. Maffezzoli, « Fabrication of a thermoplastic matrix composite stiffened panel by induction welding », *Aerosp. Sci. Technol.*, vol. 43, p. 314-320, juin 2015, doi: 10.1016/j.ast.2015.03.013.
[19] P. Sanders, « Electromagnetic welding: an advance in thermoplastics assembly », *Mater. Des.*, vol. 8, nº 1, p. 41-45, janv. 1987, doi: 10.1016/0261-3069(87)90059-8.
[20] M. J. Troughton, Éd., « Ch. 11 - Induction Welding », in *Handbook of Plastics Joining (Second Edition)*, Boston: William Andrew Publishing, 2009, p. 113-120. doi: 10.1016/B978-0-8155-1581-4.50013-5.
[21] R. Rudolf, P. Mitschang, M. Neitzel, « Induction heating of continuous carbon-fibre-reinforced thermoplastics », *Compos. Part -Appl. Sci. Manuf.,* vol. 31, p. 1191-1202, nov. 2000, doi: 10.1016/S1359-835X(00)00094-4.
[22] R. Crozier, M. Mueller, « A new MATLAB and octave interface to a popular magnetics finite element code », sept. 2016, p. 1256. doi: 10.1109/ICELMACH.2016.7732685.
[23] J. M. D. Coey, *Magnetism and Magnetic Materials*. Cambridge University Press, 2010.

[24] M. G. Vinum, M. R. Almind, J. S. Engbaek, S. B. Vendelbo, M. F. Hansen, C. Frandsen, J. Bendix, P. M. Mortensen « Dual-Function Cobalt–Nickel Nanoparticles Tailored for High-Temperature Induction-Heated Steam Methane Reforming », *Angew. Chem. Int. Ed.*, vol. 57, nº 33, p. 10569-10573, août 2018, doi: 10.1002/anie.201804832.
[25] J. Goodenough, « Summary of losses in magnetic materials », *Magn. IEEE Trans. On*, vol. 38, p. 3398-3408, oct. 2002, doi: 10.1109/TMAG.2002.802741.
[26] Chas. P. Steinmetz, « On the law of hysteresis », *Proc. IEEE*, vol. 72, nº 2, p. 197-221, févr. 1984, doi: 10.1109/PROC.1984.12842.
[27] F. J. G. Landgraf, M. Emura, M. F. de Campos, « On the Steinmetz hysteresis law », *J. Magn. Magn. Mater.*, vol. 320, nº 20, p. e531-e534, oct. 2008, doi: 10.1016/j.jmmm.2008.04.011.
[28] J. Muhlethaler, J. Biela, J. W. Kolar, A. Ecklebe, « Core Losses Under the DC Bias Condition Based on Steinmetz Parameters », *IEEE Trans. Power Electron.*, vol. 27, nº 2, p. 953-963, févr. 2012, doi: 10.1109/TPEL.2011.2160971.
[29] S. Chikazumi, *Physics of Ferromagnetism*. OUP Oxford, 2009.
[30] S. Tumanski, « Ch. 3 - Magnetic Materials », in *Handbook of Magnetic Measurements*, Routledge Handbooks Online, 2011. doi: 10.1201/b10979-4.
[31] M. Ahmadzadeh, C. Romero, J. McCloy, « Magnetic analysis of commercial hematite, magnetite, and their mixtures », *AIP Adv.*, vol. 8, nº 5, p. 056807, déc. 2017, doi: 10.1063/1.5006474.
[32] K. M. Krishnan, A. B. Pakhomov, Y. Bao, P. Blomqvist, Y. Chun,
M. Gonzales, K. Griffin, X. Ji, B. K. Roberts, « Nanomagnetism and spin electronics: materials, microstructure and novel properties », *J. Mater. Sci.*, vol. 41, nº 3, p. 793-815, févr. 2006, doi: 10.1007/s10853-006-6564-1.
[33] S. Mørup, M. F. Hansen, C. Frandsen, « Magnetic Nanoparticles », in *Comprehensive Nanoscience and Technology*, vol. 1, 2011, p. 433-487. doi: 10.1016/B978-0-12-374396-1.00036-2.
[34] E. F. Kneller, F. E. Luborsky, « Particle Size Dependence of Coercivity and Remanence of Single-Domain Particles », *J. Appl. Phys.*, vol. 34, p. 656-658, mars 1963, doi: 10.1063/1.1729324.
[35] J. S. Lee, J. Cha, H. Yoon, J.-K. Lee, Y. K. Kim, « Magnetic multi-granule nanoclusters: A model system that exhibits universal size effect of magnetic coercivity », *Sci. Rep.*, vol. 5, p. 12135, juill. 2015, doi: 10.1038/srep12135.
[36] W. D. Callister, *Materials Science and Engineering: An Introduction*. Wiley, 1997.
[37] E. F. Westrum, F. Grønvold, « Magnetite (Fe3O4) Heat capacity and thermodynamic properties from 5 to 350 K, low-temperature transition », *J. Chem. Thermodyn.*, vol. 1, nº 6, p. 543-557, nov. 1969, doi: 10.1016/0021-9614(69)90015-9.
[38] Testo SE & Co., « Thermography Pocket Guide ». 2017. Consulté le: avr. 09, 2021. [En ligne]. Disponible sur: https://static-int.testo.com/media/1d/b7/21fc65abbea1/Pocket-Guide-Thermography-EN.pdf
[39] G. Wilson, « 13 - Slurry Pumps », in *Centrifugal Pumps (Second Edition)*, V. S. Lobanoff et R. R. Ross, Éd. Boston: Gulf Professional Publishing, 1992, p. 226-245. doi: 10.1016/B978-0-08-050085-0.50016-3.
[40] « The hardness of metals: a visual representation of the Mohs scale for mettalic elements and alloys ». Alan's factory Outlet. Consulté le: mai 05, 2021. [En ligne]. Disponible sur: https://www.sccboe.org/cms/lib/AL50000450/Centricity/Domain/779/the-hardness-of-metals-a-visual-representation-of-the-mohs-scale.pdf
[41] S. Wahyuningsih, A. Ramelan, et Y. Kristiawan, « Transformation of Magnetite (Fe3O4) and Maghemite (γ–Fe2O3) to α–Fe2O3 from Magnetic Phase of Glagah Iron Sand », *J. Eng. Sci.*, vol. 15, p. 11-21, mai 2019, doi: 10.21315/jes2019.15.2.
[42] H. Shokrollahi, « A review of the magnetic properties, synthesis methods and applications of maghemite », *J. Magn. Magn. Mater.*, vol. 426, p. 74-81, mars 2017, doi: 10.1016/j.jmmm.2016.11.033.

R. G. Martin, C. Johansson, J. R. Tavares, M. Dubé*

Material Selection Methodology for an Induction Welding Magnetic Susceptor based on Hysteresis Losses

This study presents a method to select magnetic particles that act as a magnetic susceptor relying on hysteresis losses for induction welding. The critical material properties and the governing equation are presented. The methodology is then applied to a case study in which iron, nickel and magnetite are evaluated to be used for heating and melting polypropylene and poly-ether-ether-ketone.

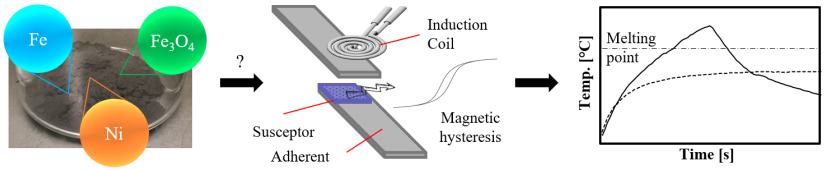

Supporting Information

Material Selection Methodology for an Induction Welding Magnetic Susceptor based on Hysteresis Losses

*Romain Georges Martin, Christer Johansson, Jason Robert Tavares, Martine Dubé**

Modelling of the magnetic field around an induction coil is performed using FEMM4.2 software. The section of the hairpin coil (straight and single-turn coil) is simplified as a 6 x 6 mm square with a 4 x 4 mm square hole inside of it, where the cooling water is circulating. The two square sections are separated by 6.4 mm. The magnetic field concentrator is simplified as a 12.6 mm high and 32 mm wide rectangle, surrounding the coil sections. The materials are defined as following: air for the surrounding space and for the inside of the coil (water can be approximated as air in terms of magnetic response), copper for the coil section and Ferrotron 559H for the field concentrator. As this latter is not available in the software materials library, it is created following the material technical datasheet. The current inside the copper coil sections is fixed at 700 A. The current must be positive in one of the two sections and negative in the other, as the induction coil is a closed loop. The default Dirichlet boundary condition is used in the simulations.